Coordinated Wide-Area Control of Multiple Controllers in a Power System Embedded with HVDC Lines

Pooja Gupta, Student Member, IEEE, Anamitra Pal, Senior Member, IEEE, and Vijay Vittal, Fellow, IEEE

Abstract—This paper develops a coordinated wide-area control of power system stabilizers (PSSs), static VAr compensators (SVCs), and supplementary damping controllers (SDCs) for damping low frequency oscillations (LFOs) in a power system embedded with multiple high voltage DC (HVDC) lines. The improved damping is achieved by designing a coordinated widearea damping controller (CWADC) that employs partial state feedback. The design methodology uses a linear matrix inequality (LMI)-based mixed H_2/H_{∞} robust control for multiple operating scenarios. To reduce the high computational burden, an enhanced version of selective modal analysis (SMA) is employed that not only reduces the number of required wide-area feedback signals, but also identifies alternate feedback signals, in case of failure of the primary signals. Additionally, the impact of delays on the performance of the control design is investigated. The studies are performed on a 29 machine, 127 bus equivalent model of the Western Electricity Coordinating Council (WECC) systemembedded with three HVDC lines and two wind farms.

Index Terms—Coordinated Wide-Area Damping Controller (CWADC), High Voltage Direct Current (HVDC), Linear Matrix Inequality (LMI), Partial state feedback, Phasor Measurement Unit (PMU), Polytopic control, Selective Modal Analysis (SMA)

I. INTRODUCTION

RADITIONALLY, low frequency oscillation (LFO) damping in a power system is provided by power system stabilizers (PSSs) installed at generator units. However, the PSSs have to be carefully tuned to damp both local plant modes as well as inter-area modes. HVDC systems, which are primarily used for power delivery, can improve power system stability by rapidly altering their power flows. Addition of supplementary damping controllers (SDCs) to flexible alternating current transmission system (FACTS) devices have also proven to be effective for damping oscillations [1]. However, as power systems experience a wide range of variations in loads, generations, and configurations, controllers designed to work in *isolation* may not be effective in damping the frequencies observed under diverse scenarios.

The deployment of phasor measurement units (PMUs) has increased the accessibility to time-synchronized wide-area measurements, which has, in turn, enabled the effective detection and control of power swing modes [2], [3]. The use of PSSs for damping inter-area oscillations based on remote measurements has been explored in [4], [5]. The implementation of FACTS devices using feedback from remote measurements

Pooja Gupta is currently a Ph.D. student at Arizona State University, Tempe, AZ-85287 (e-mail:pgupta69@asu.edu).

Anamitra Pal is an Assistant Professor at Arizona State University, Tempe, AZ-85287 (e-mail:anamitra.pal@asu.edu).

Vijay Vittal is a Professor at Arizona State University, Tempe, AZ-85287 (e-mail:vijay.vittal@asu.edu).

was investigated in [6], [7]. An actual application of wide-area measurements to damp inter-area oscillations via modulation of active power of the Pacific DC Intertie (PDCI) was presented in [8]. In [9]–[13], wide-area coordinated control of energy storage devices (ESDs), PSSs, HVDC lines, and static VAr compensators (SVCs) was proposed. However, most of these control design schemes suffered from at least one of the following shortcomings: a) the controllers needed to be tuned for different operating conditions, which was a concern for power systems engineers in terms of required computational time to first analyze and then initiate corrective action, and b) proposed designs were higher-order controllers, which were too complicated for actual implementation on larger and more realistic systems.

To address the aforementioned issues, a control technique is proposed in this paper to *simultaneously* coordinate different types of damping controllers. This strategy combines the advantages provided by local signals with the additional degrees of freedom provided by remote measurements to achieve the targeted damping of LFOs. Additionally, since it is preferable that feedback signals are synthesized from a small set of measurements, the proposed work exploits the dynamic characteristics of oscillatory modes to first choose an optimal number of state feedback signals and then design an optimally coordinated wide-area controller for a range of scenarios using partial state feedback. Lastly, to make the wide-area measurements-based design robust against communication latencies and loss of remote signals, an alternate feedback selection technique is developed.

The designed controller is composed of gains that are determined by solving a convex optimization problem that minimizes the weighted sum of the H_2/H_∞ controls while satisfying the pole-placement constraints, to i) improve the interactions among the controllers, and ii) attain a desired level of damping for the closed loop system. The salient contributions of the paper are:

- a) evaluation of the improvement in the small-signal stability that HVDC based SDC (DC-SDC) can achieve,
- b) use of detailed standard dynamic models of controllers such as PSSs and SVCs, to accurately determine the interactions between the controls and the network,
- c) development of a robust CWADC for a reduced-order polytopic system using LMI-based mixed H_2/H_∞ control with partial state feedback and regional pole placement constraints.
- d) systematic study of the impact of communication delays on the proposed approach, and
 - e) identification of alternate feedback signals for CWADC.

II. CONTROLLERS AND THEIR INTERACTIONS

1) Design of PSSs, SVCs and DC-SDCs: The aim of both PSSs and DC-SDCs is to damp the modes of rotor oscillations by inducing pure damping torques on shafts of generators. The PSS model shown in Fig. 1(a) uses shaft speed deviation as an input signal to add the stabilizing signal, V_s^{PSS} , to the exciter input and is of the form,

$$V_s^{PSS} = K_{PSS}(\frac{sT_w}{1 + sT_w})(\frac{1 + sT_{1PSS}}{1 + sT_{2PSS}})(\frac{1 + sT_{3PSS}}{1 + sT_{4PSS}})\Delta\omega$$
(1)

The design of DC-SDC used in this work is similar to the conventional structure of a PSS as shown in Fig. 1(b). The controller output, P_{mod}^{DC} , given by (2), modulates the active power reference setpoint through the HVDC link based upon the local signal, i.e., the frequency deviation of the AC bus to which the DC converter is connected.

$$P_{mod}^{DC} = K_{DC} \left(\frac{sT_w}{1 + sTw}\right) \left(\frac{1 + sT_{1DC}}{1 + sT_{2DC}}\right) \left(\frac{1 + sT_{3DC}}{1 + sT_{4DC}}\right) \Delta f \tag{2}$$

The first terms after the gain in (1) and (2) are used to washout the compensation effect after a time lag, T_w , which ensures that steady state changes in the input do not modify the output signal. $T_{1PSS} - T_{4PSS}$ are lead time constants for PSSs to compensate the phase lag between the input and output signals at oscillation frequencies of interest, and $T_{1DC} - T_{4DC}$ are lead compensation pairs for DC-SDCs. K_{PSS} represents the gain block for PSS, while K_{DC} is the gain for DC-SDC. The third type of controller which is considered in this study is an SVC whose structure is shown in Fig. 1(c). Although its primary objective is to provide voltage support to the system, it is equipped with the additional capability of responding to wide-area signals to damp LFOs of interest. It is worth noting that the selection of control structures and input signals for the three types of controllers used in this paper are based on the standard models given in [8], [12], [14], [15].

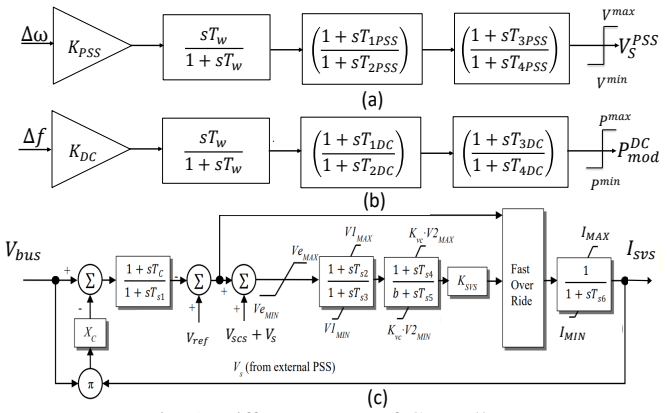


Fig. 1. Different Types of Controllers.

2) Types of Control Interactions: To enhance the performance of large interconnected power systems, there has been a considerable increase in the number and complexity of power system controllers. However, the inter-controller interactions may result in effects that are detrimental to the overall system performance. As there can be many possible combinations and configurations of the controls, the scope of this paper is limited to the study of interactions between the following controllers in the electromechanical frequency ranges:

- a) Interactions between different PSSs,
- b) Interactions between PSSs and SVCs.
- c) Interactions between PSSs, SVCs, and DC-SDCs.

2

These interactions can manifest themselves in many ways. For example, improvement in the gain of DC-SDC can improve the damping of one mode, but degrade the damping of other modes. Hence, there is a need to coordinate the tuning of these controls. Although the study system in this work contains PSSs, SVC, and DC-SDC, the presented technique is also applicable to other devices, such as ESDs.

III. PROPOSED WIDE-AREA DAMPING CONTROLLER STRUCTURE

One way to provide better observability of the inter-area modes of oscillation as well as minimize the potential for adverse interactions among the (multiple) existing controllers is by using both local and wide-area signals simultaneously, resulting in a bi-level operational scheme. The selected stabilizing signals are measured by geographically distributed PMUs and sent to the CWADC through dedicated communication links. The control signals are then sent to automatic voltage regulators (AVRs) of selected machines, SDCs installed on DC lines, and SVCs as shown in Fig. 2. On receiving the respective control commands, the controllers act in unison to increase the damping of oscillation modes. This design process does not require any modification of the parameters of the existing controllers; instead, it exerts additional stabilizing signals, u_i , (where $i = \{1, 2, ...p\}$; p < total controllers) to enable them to overcome their tuning deficiencies. Furthermore, if remote signals are lost, the bi-level design ensures that all the controllers can work autonomously based on the locally available information.

To restrict the output of the CWADC within an acceptable range, limiters are also included. Limiter action is mandatory as the proposed controller can create unnecessary violations in the AC and DC voltages of the network due to the action of local controllers. In this design process, all PSSs, DC-SDCs, and SVCs are modeled in the open-loop state-space representation, on which the design of CWADC is based.

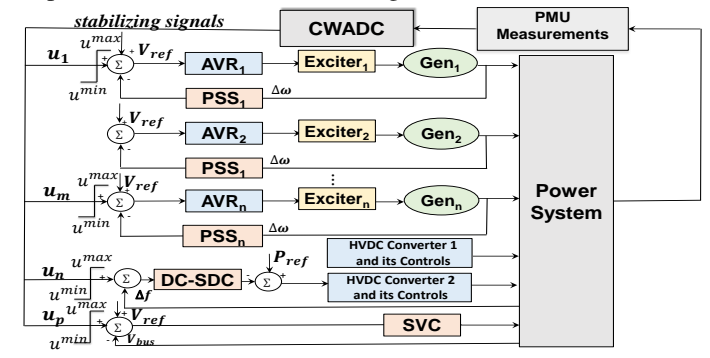


Fig. 2. Input/Output Control Scheme for Bi-level Design.

A. Multi-objective H_2/H_{∞} Controller Design

An ideal control design must satisfy a mix of performance and robustness objectives, which can be difficult to realize using a single control criterion [16], [17]. Therefore, the proposed controller is designed based on a multi-objective H_2/H_∞ synthesis technique, that incorporates various criteria including control effort minimization, disturbance rejection,

optimal control performance, and control robustness. The H_2 optimization gives more control over the system's transient behavior while minimizing control cost, while the H_∞ control ensures robustness against dynamic uncertainties [18]. To ensure good transient response of the closed-loop system, poleplacement constraints are added to the multi-objective control problem. Such constraints are important as they keep gains at reasonable values, which may otherwise lead to controller output saturation [3]. An LMI framework is used to solve for state feedback with the combination of objectives described above. The state-space model of the studied system and its associated controls corresponding to an operating condition (OC) posed with H_2/H_∞ formulation is described by:

$$\dot{x} = Ax + B_1 w + B_2 u
z_{\infty} = C_1 x + D_{11} w + D_{12} u
z_2 = C_2 x + D_{22} u
y = C_y x + D_{y1} w + D_{y2} u$$
(3)

where x is the state of the system, u is the control, w is the disturbance, y is the output, A, B_1 , B_2 , C_1 , C_2 , D_{11} , D_{12} , D_{22} , C_y , D_{y1} , D_{y2} are state-space matrices, and z_2 and z_∞ correspond to H_2 and H_∞ controls, respectively. Note that D_{21} is set to zero for computing the optimal H_2 control, as it will otherwise make the H_2 norm infinite. Now, the LMI problem corresponding to H_2/H_∞ constraints for this OC can be formulated as:

$$\begin{bmatrix} AX + XA^{\mathrm{T}} + B_{2}Y + Y^{\mathrm{T}}B_{2}^{\mathrm{T}} & B_{1} & XC_{1}^{\mathrm{T}} + Y^{\mathrm{T}}D_{12}^{\mathrm{T}} \\ B_{1}^{\mathrm{T}} & -I & D_{11}^{\mathrm{T}} \\ C_{1}X + D_{12}Y & D_{11} & -\gamma^{2}I \end{bmatrix}$$
(4)

$$< 0$$

$$\begin{bmatrix}
Q & C_2X + D_{22}Y \\
XC_2^{\mathrm{T}} + Y^{\mathrm{T}}D_{22}^{\mathrm{T}} & X
\end{bmatrix} > 0$$
 (5)

where X is the Lyapunov matrix, Q is a positive-definite matrix, \otimes is the Kronecker product, Y = KX, $\gamma^2 < \gamma_\infty^2$ and $\operatorname{Trace}(Q) < \gamma_2^2$. γ_2 and γ_∞ are maximum bounds for closed-loop transfer functions of system for H_2 and H_∞ controls, respectively. LMI regions are convex subsets of the complex plane, and can be described by $D = s \in \mathbb{C}$: $V + Ws + W^T \overline{s} < 0$, where \mathbb{C} refers to the complex plane, $V = V^T$ and W are fixed real matrices, and \overline{s} is the complex conjugate of s. Different complex regions in the complex planes that are symmetric with respect to the real axis, such as half plane, conic sectors, circles, as well as their combinations, can be expressed as LMI regions. Lastly, the closed-loop system will be D-stable if and only if there exists a positive definite matrix, X, such that [17]

$$(V \otimes X) + (W \otimes (AX + B_2Y)) + W^{\mathsf{T}} \otimes (AX + B_2Y)^{\mathsf{T}} < 0 \quad (6)$$

B. Polytope Formation

Power system OCs vary with system configuration and load in a complex manner. As the system's OC changes, the characteristics of the oscillation modes also vary. A controller designed for the nominal OC of a network may not work optimally for an actual OC, which is influenced by factors such as load variations, availability of renewable generation, tie-line outages, and energy market fluctuations. It therefore,

makes more sense to combine different OCs together to design a single damping controller that is effective over a *convex combination* of those OCs. To successfully develop such a control, this paper proposes creating an LMI-based polytopic control design, in which the uncertainty of the system is incorporated in the design. For implementing such a control, the system is linearized at a number of typical OCs that are decided by the scheduling variables measurable in real-time, such as load levels and tie-line flows. The OCs with converged power flows constitute the vertices of the polytope. For a given OC, the vertex, v of the polytope, Γ , can be expressed as:

$$\Gamma_{v} = \begin{bmatrix}
A_{v} & B_{v1} & B_{v2} \\
C_{v1} & D_{v11} & D_{v12} \\
C_{v2} & 0 & D_{v22} \\
C_{vy} & D_{vy1} & D_{vy2}
\end{bmatrix}$$
(7)

The convex combination of different vertices representing different system matrices is given by:

$$\Gamma\{\Gamma_1, \Gamma_2, ... \Gamma_v\} = \{\sum_{i=1}^v \alpha_i \Gamma_i : \sum_{i=1}^v \alpha_i = 1, \alpha_i \ge 0\}$$
 (8)

Here, α_i denotes the polytopic coordinate of Γ . The convexity property of the polytope ensures that once the quadratic stability is established for the vertices, the same control extends for the complete polytope.

C. System Reduction

With detailed machine models and their controls (such as exciters, PSSs, governors, HVDC controllers, and SVCs), the size of A_v and Γ_v as defined in (7) can become large even for a moderately sized system. As such, to reduce the complexity of implementation, it is desirable to obtain a lower order plant model. In this research, selective modal analysis (SMA) [19] is used for simplifying the complicated linear timeinvariant (LTI) models of the dynamic system, as it provides the advantage of retaining the physical attributes of the state variables that are strongly linked to LFOs. Furthermore, as the identity of the state variables is known a priori, SMA can be used to exploit the state clustering and coherency techniques [20], [21]. A rigorous comparison of the full and reducedorder systems using modal analysis has ensured that only those system states that have little effect on the input-output behavior of the system are discarded [13].

D. Selection of Control and Stabilizing Signals

Measurements that are associated with inter-area oscillations are good choices for stabilizing signals. A methodology for selecting a suitable set of relevant measurements was introduced in [13] where SMA in conjunction with the modified participation factors (PFs) (obtained after scaling the original PFs for each state with respect to the generator's average contribution in all the system modes) and k-means clustering were used to evaluate the strength of candidate signals with respect to LFO modes. The method (referred to as *enhanced SMA*) helped in: a) distinguishing the set of critical generators from non-critical generators, and b) designing a partial state feedback control for the complete system using *only* the critical generator set. The wide-area input stabilizing signals used in this paper are angles and speeds of critical generators

obtained after performing enhanced SMA, since they provide a reasonably good approximation to the frequencies of swing modes. For the highest controllability of these modes, the CWADC sends the control signals to the SVC, DC-SDC, and exciters of the generators belonging to the critical set, which together constitute the second control level in the bilevel closed-loop control system. The PSSs belonging to the non-critical set of generators remain fully decentralized.

The control law for the LMI polytopic controller with gain matrix, $K_{LMI-poly}$, is given by $u = K_{LMI-poly}x_l$, where

$$K_{LMI-poly} = \begin{bmatrix} K_{11} & K_{12} & K_{13} & \dots & K_{1l} \\ K_{21} & K_{22} & K_{23} & \dots & K_{2l} \\ \dots & \dots & \dots & \dots \\ K_{i1} & K_{i2} & K_{i3} & \dots & K_{il} \end{bmatrix}$$
(9)

where x_l denotes the reduced number of states obtained using the enhanced SMA, while i signifies the number of controls present in the system.

IV. STUDY SYSTEM

A reduced-order model of the WECC that includes the modeling features and complexities of the actual system (such as the inter-area modal properties) is used to demonstrate the performance of the CWADC. The test system is shown in Fig. 3. This system has 33 synchronous generator units, 140 buses, and 2 wind farms. All synchronous machines are represented in detail using a two-axis model, type ST1 excitation control, and general-purpose turbine-governor models. They also have conventional, local PSSs as shown in Fig. 2. All loads are of the constant impedance type. The two wind farms are installed at bus #9991 and bus #8881, and are represented using Type 3 WTG and control modules. The system also has three HVDC lines, two of which represent the multi-terminal HVDC lines, the Pacific DC Intertie (PDCI) between Celilo and Sylmar substations transmitting 2,300 MW from the Northwest to the Southwest under normal conditions; the third one is the Intermountain Power Project (IPP), which transmits 1,750 MW from the Mideast to the Southwest region of the WECC. The PDCI and IPP were modeled as simple positive and negative loads in [13], but they are modeled using detailed dynamic models in this study. SDC is added to one of the two multiterminal DC lines, whose model along with that of SVC are shown in Fig. 2. The rating of the SVC is 100 MVAr. Based on [8], the modulation limit for DC-SDC is set to ± 125 MW. All existing generator excitation controls along with DC-SDC and SVC in the system are assumed to contain a communication module to accept control signals from the CWADC.

A. Setting up of Polytopic Region

The proposed controller is intended to not only prevent negative interactions between different controllers, but also enhance the damping of multiple oscillation modes that may appear in a wide range of operating conditions. In this study, seven different OCs with converged powerflow solutions are analyzed, as shown in Table I, and combined into a single polytope. To obtain these operating points, power generation and load demands are varied at the selected generator and load buses resulting in changes in power transfers in and around WECC Intertie Path #26 [22]. To ascertain if the designed

polytopic controller can damp unstable oscillation modes, one of the OCs (vertex v_6) had a converged powerflow solution, but an unstable open-loop mode (see Table II).

TABLE I. Test Cases

Case/	Parameter Variation		
Vertex No.	Generation	Load	
v_1	No Change	No Change	
v_2	#91-Increase by 250 MW	#71-Increase by 250 MW	
v_3	#91-Decrease by 500 MW	#71-Decrease by 500 MW	
v_4	#8881-Increase by 250 MW	#69-Increase by 250 MW	
v_5	#8881-Decrease by 500 MW	#69-Decrease by 500 MW	
	#91-Increase by 200 MW		
v_6	#8881-Increase by 200 MW	#78-Increase by 400 MW	
	#91-Decrease by 250 MW		
v_7	#8881-Decrease by 250 MW	#78-Decrease by 500 MW	

Small-signal stability analysis of the full system at each of the seven vertices reveals multiple LFO modes with poor damping ratios (< 5%). Table II shows three of the least damped modes obtained for the studied system. The system eigenvalues, damping ratios, and PFs at each of these OCs are computed using the SSAT software [23].

The impact of negative interactions among different controls on the damping of one of the critical modes of the system is shown in Table III. It can be seen that PSS and SVC which together add at least 3.46% damping to Mode1 for vertices v_2 and v_6 , have interacted negatively with the DC-SDC, reducing its damping to less than 1%. In particular, Mode1 has become unstable for vertex v_6 due to the inter-controller interactions.

TABLE II. Damping of Selected Modes

Case	Damping of critical modes(%)			
No.	Mode 1	Mode 2	Mode 3	
v_1	3.71% @1.737Hz	4.03% @0.934Hz	4.14% @1.115Hz	
v_2	0.27% @0.397Hz	2.46% @0.768Hz	2.98% @0.923Hz	
v_3	3.74% @1.736Hz	4.05% @0.939Hz	4.07% @1.117Hz	
v_4	3.63% @1.742Hz	4.04% @0.926Hz	4.08% @1.114Hz	
v_5	3.71% @1.737Hz	4.03% @0.934Hz	4.14% @1.115Hz	
v_6	-0.36% @0.399Hz	2.39% @0.766Hz	2.97% @1.743Hz	
v_7	3.23% @0.430Hz	3.36% @0.787Hz	3.47% @1.206Hz	

TABLE III. Negative Controller Interactions

Case	Critical Mode	Damping(%)	
No.	from Table I	PSS + SVC	DC-SDC + PSS + SVC
v_1	Mode1	3.51	3.71
v_2	Mode1	3.47	0.27
v_3	Mode1	3.54	3.74
v_4	Mode1	3.42	3.63
v_5	Mode1	3.51	3.71
v_6	Mode1	3.46	-0.36
v_7	Mode1	3.49	3.23

B. System Reduction

The size of the A and B matrices for each vertex is 656 \times 656 and 656 \times 35, respectively. Here, 35 refers to the total number of damping controllers present in the system, i.e. 33 PSSs installed at all synchronous machines, 1 DC-SDC, and 1 SVC. Every controller is tuned to provide minimum damping of 3% at the base OC. With the help of the enhanced SMA and modified PFs approach described in [13], the size of the A matrix for each of the seven OCs is reduced to 43 \times 43 (speeds of the 22 machines (including reference machine) and angles of 21 machines computed with respect to the reference machine). The performance of the enhanced SMA used for obtaining the reduced A matrices for two OCs is shown in Figs. 4-IV-C. The black dots represent the eigenvalues of the complete system, while the black circles

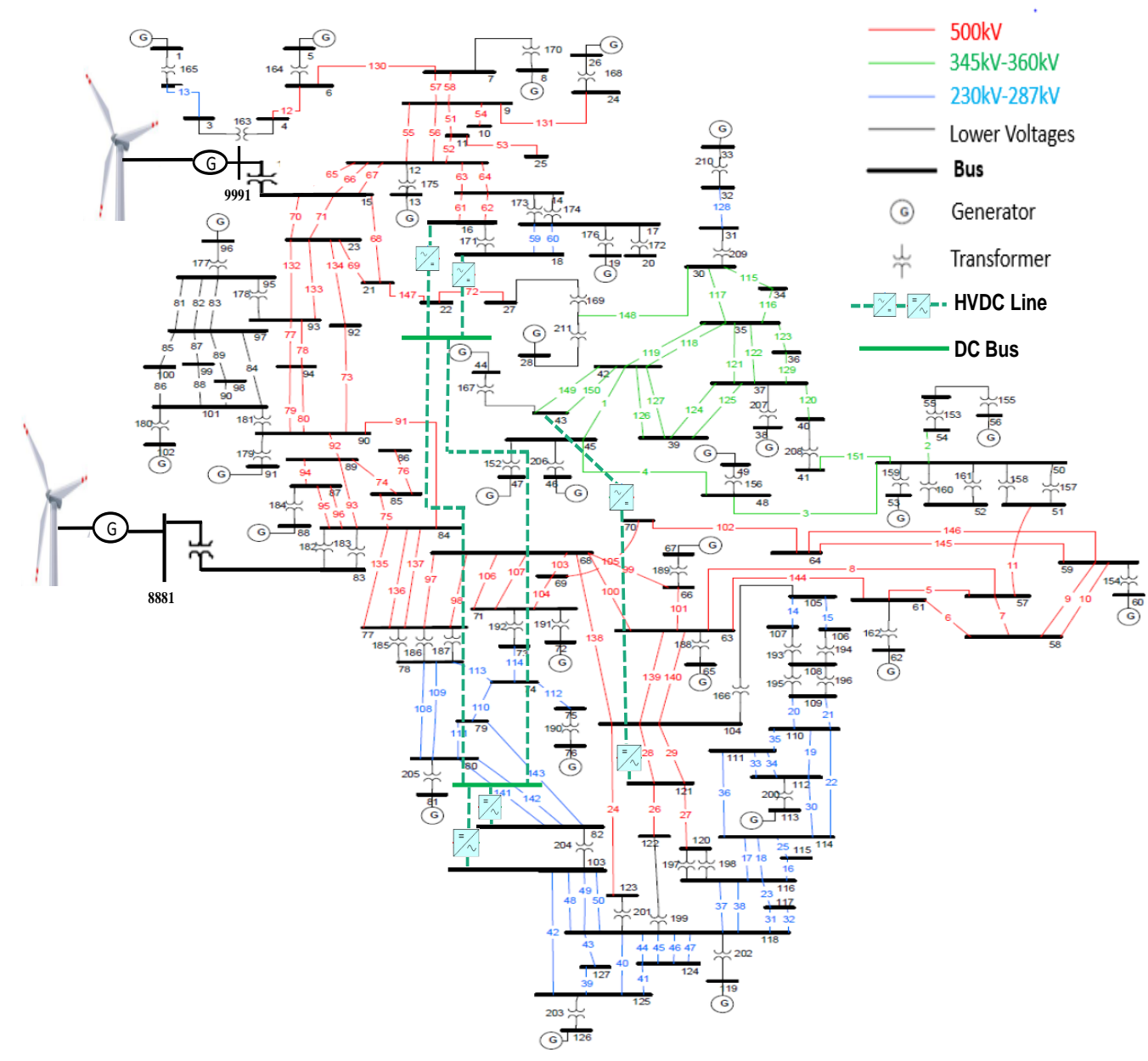


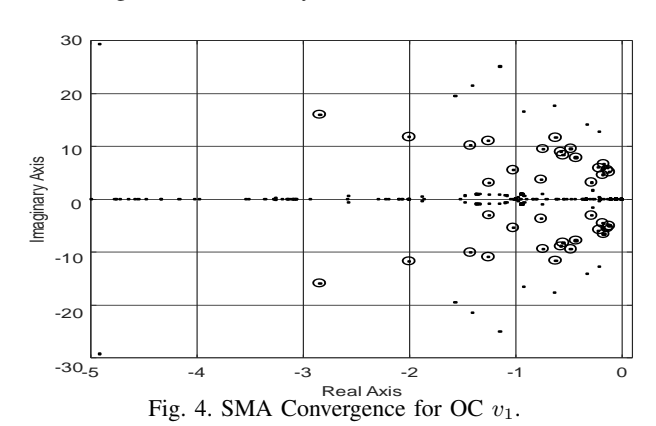
Fig. 3. Reduced-Order WECC Model.

represent the eigenvalues of the reduced-order system. The size of the B matrix is reduced to 43 \times 24, where 24 signifies the number of controllers that are part of CWADC. The remaining 11 controllers belong to a set of non-critical generators as explained in Section III-D. Each LMI problem with 43 retained states is described by a 66 \times 92 LTI system. The collection of seven vertices results in a 69 \times 652 polytopic system.

C. Synthesis of CWADC

To develop the LMI based mixed H_2/H_∞ control for the polytopic system with regional pole-placement constraints, the msfsyn function available in the LMI control toolbox of MATLAB was used [17]. The size of the designed controller gain matrix, $K_{LMI-poly}$ is 24 \times 43, hence CWADC is a 43-input, 24-output system. To guarantee the system's performance over a wide range of operating points, the proposed CWADC gathers system-wide measurements from geographically diverse locations in WECC. This ensures the availability

of more system dynamic information contained in remote stabilizing signals. It is to be noted that though the CWADC is designed for the reduced-order system, its performance is tested using the full-order system.



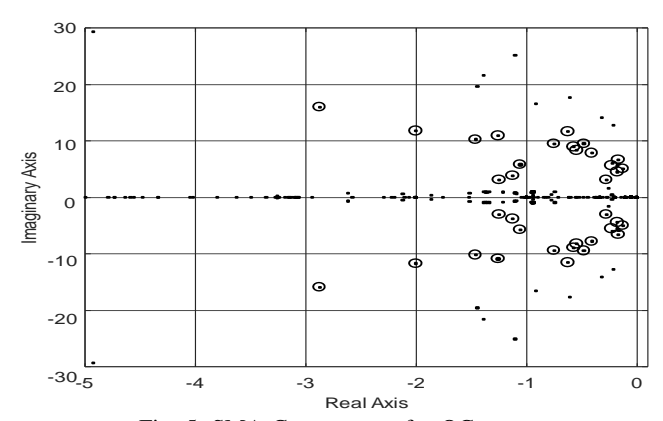


Fig. 5. SMA Convergence for OC v_2 . V. APPLICATION OF THE PROPOSED CONTROL SCHEME

A. Performance of the CWADC

Table IV shows the application of the LMI control design for the polytopic system. All the critical eigenvalues including those listed in Table II, have attained minimum damping, ζ_{min} , of 5.5%. It was also observed that at higher load conditions, with the CWADC included, the power flow in and around the WECC Intertie Path #26 could be increased. Specifically, the system's stability limit was extended from 3,398 MW to 3,598 MW (increase in load at bus #71 from 300 MW to 500 MW), 1,830 MW to 1,930 MW (increase in load at bus #69 from 600 MW to 700 MW), and 1,616 MW to 1,741 MW (increase in load at bus #78 from 550 MW to 675 MW), respectively, for vertices v_2 , v_4 , and v_6 specified in Table I. It should be noted that for vertices v_2 and v_4 , the limit is imposed by the powerflow not converging beyond these values.

TABLE IV. Results of the Modal Analysis

Case	Damping of critical modes(%)				
No.	Mode 1	Mode 2	Mode 3		
v_1	9.19% @1.71Hz	5.51% @0.964Hz	5.70% @1.14Hz		
v_2	12.54% @0.427Hz	12.5% @0.75Hz	5.68% @0.96Hz		
v_3	10.6% @1.71Hz	5.59% @0.96Hz	5.91% @1.15Hz		
v_4	13.69% @1.71Hz	5.64% @0.95Hz	6.04% @1.15Hz		
v_5	9.23% @1.71Hz	5.57% @0.96Hz	5.96% @1.15Hz		
v_6	12.85% @0.41Hz	9.54% @0.76Hz	9.38% @1.707Hz		
v_7	11.92% @0.45Hz	11.51% @0.76Hz	9.48% @1.24Hz		

To evaluate the performance of the CWADC, the results obtained using modal analysis are validated by conducting nonlinear time-domain simulations in PSLF [15]. A small disturbance is created by simultaneously increasing load at bus #78 by 200 MW and decreasing load at bus #71 by 400 MW at time, t = 0.5sec. Note that although this OC lies inside the polytope, it does not coincide with the vertices. The active power responses of three different generators, namely, generators at buses #5, #76, and #91, that have higher participation in the inter-area modes (shown in Table II), are shown in Figs. 6-8, with and without CWADC (i.e. in the presence of local controllers (PSSs, DC-SDC, and SVC) only). It can be seen that the CWADC is able to improve the damping of the inter-area modes present in the full-order system; for example, oscillation frequencies such as 1.2Hz, 0.75Hz, and 1.7Hz identified through Prony analysis of the plots showed damping of 5.4%, 7.8%, and 10.2%, respectively. Figs. 9-10 show the control efforts extended by the DC-SDC and SVC, both of which are within their predefined limits.

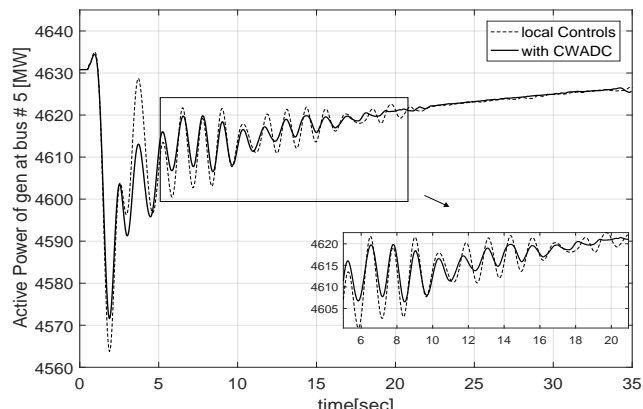


Fig. 6. Active Power of Generator at Bus#5.

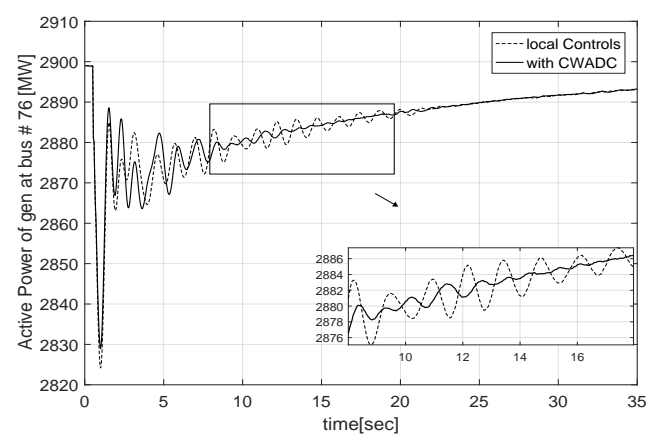


Fig. 7. Active Power of Generator at Bus#76.

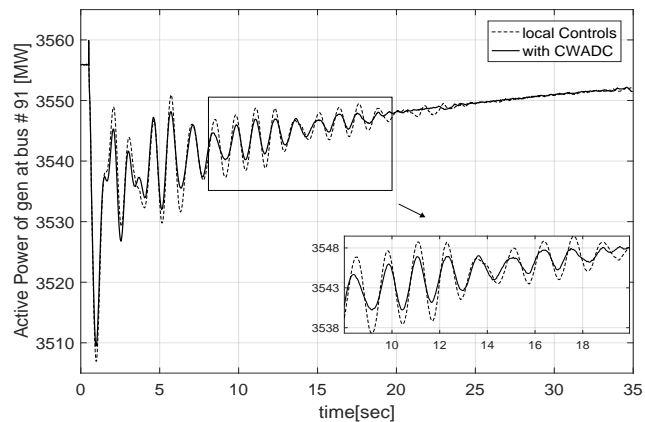


Fig. 8. Active Power of Generator at Bus#91.

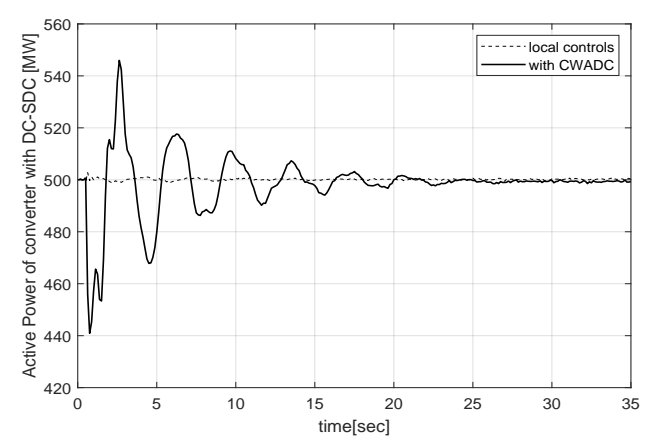


Fig. 9. DC Power of one of the Converters of the PDCI.

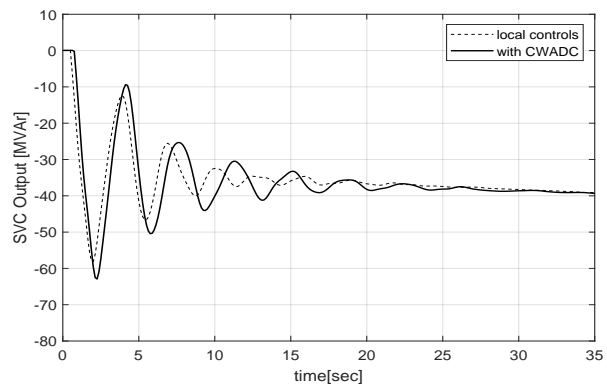


Fig. 10. Reactive Power injected by SVC.

B. Flexibility of Selecting Control Signals

The assessment of the performance of CWADC demonstrates that the use of wide-area signals can improve the system's stability. However, the performance of the CWADC may deteriorate when the quality of PMU data is poor, e.g., due to PMU device failure and/or communication failure. To ensure reliable access to PMU signals, an alternate feedback selection scheme is integrated into the proposed control design.

The selection of the alternate feedback control signals is performed based on Algorithm II of [13], which is briefly summarized below. To select an alternate set of control signals, a set $\Phi = \Psi_{non-crit}^{init} \setminus \Psi_{non-crit}^{final}$ is defined, where $\Psi_{non-crit}^{init}$ denotes the initial set of non-critical generators identified using k-means clustering and modified PFs, while $\Psi_{non-crit}^{final}$ signifies the primary set of non-critical machines that are dropped from the control group using enhanced SMA. With the help of an iterative process, a single generator in the list of non-critical generators, $\Psi_{non-crit}^{final}$ is replaced with a generator belonging to Φ , and the system that is composed of generators other than that belong to $\Psi_{non-crit}^{final}$, is tested for two conditions, namely, convergence of SMA and a stable closed-loop system after the application of a linear quadratic control (LQR) control (which is a special case of H_2 control). If the system satisfies these two conditions, then the retained group of machines that result in a stable and converged system form the alternate control set of critical generators, Ψ_{crit}^{alt} On comparing the primary set of critical generators, Ψ_{crit}^{prim} , with Ψ_{crit}^{alt} , it is observed that the two sets have identical elements except one. The new element in Ψ^{alt}_{crit} serves as an alternate location for taking the feedback in case the PMU at the corresponding generator in Ψ^{prim}_{crit} encounters a problem. Applying this process iteratively, multiple sets of alternate feedback signals can be generated.

On applying this algorithm to the system under investigation, it is found that the generator present at bus #113 is a reliable alternate to the generator at bus #67. Using this alternate set of feedback signals, the CWADC was redesigned for the OCs shown in Table I. The size of the controller gain matrix, $K_{LMI-poly}$ is 23 \times 41. This is smaller in size compared to the one obtained using the primary set of feedback signals because there are two generator units installed at bus #67, both of which are now dropped from the control set. Fig. 11 provides the result for the LMI control obtained using the alternate feedback signal. It can be realized that all the critical eigenvalues shown in black oval, including

the ones given in Table II, have attained ζ_{min} of 5.5%. The active power variations for the three generators shown in Section V-A are plotted in Figs. 12-14. From the plots, it is confirmed that the use of the alternate feedback signals has the same impact on the system's damping as the signals from the primary set. The outputs of the DC line and the SVC, modulated as a result of the supplementary stabilizing signals from the CWADC are shown in Figs. 15-16.

This simulation confirms that if the PMU at bus #67 is out of service, the proposed controller can obtain a feedback signal from the PMU at bus #113 to generate an equivalent feedback control. That is, backup observability of generator at bus #67 (a generator in Nevada) is ensured by the PMU at bus #113 (a generator in Southern California), and vice-versa (see Fig. 3). However, it must be pointed out that it may not be possible to find a suitable replacement for every critical generator in the primary set. Therefore, if PMUs at many locations fail simultaneously, the designed controller may not be able to provide requisite damping for all the OCs.

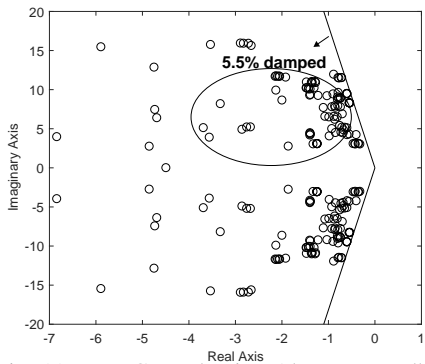


Fig. 11. LMI Control using Alternate Feedback.

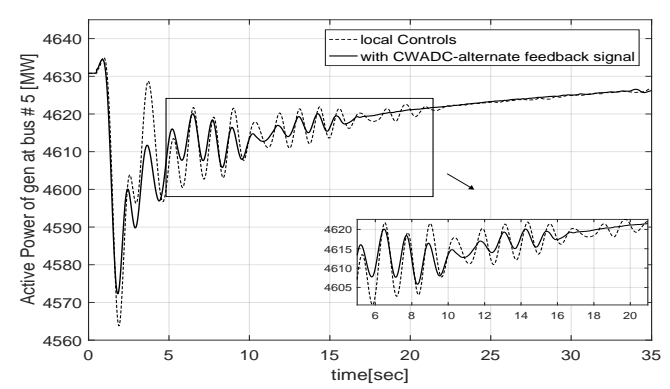


Fig. 12. Alternate Feedback-Active Power of Generator #5.

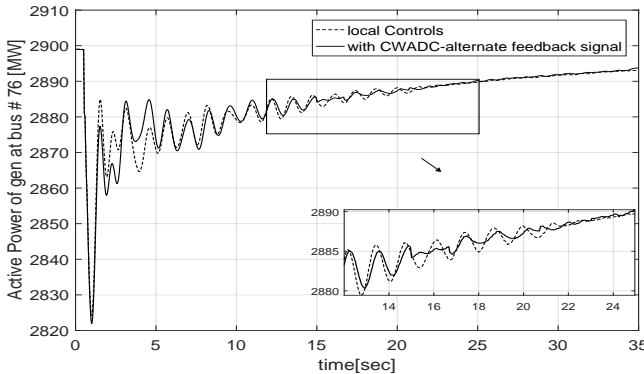


Fig. 13. Alternate Feedback-Active Power of Generator #76.

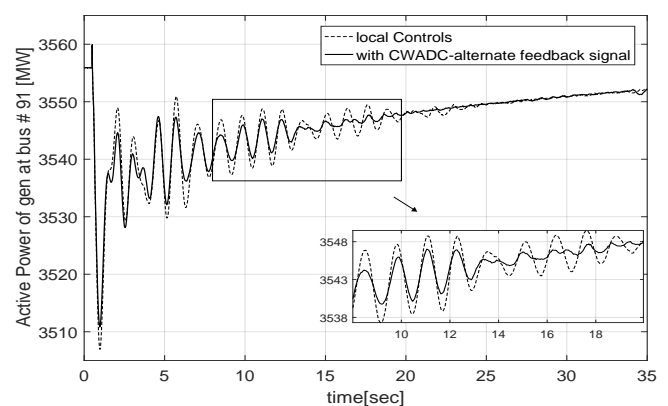


Fig. 14. Alternate Feedback-Active Power of Generator #91.

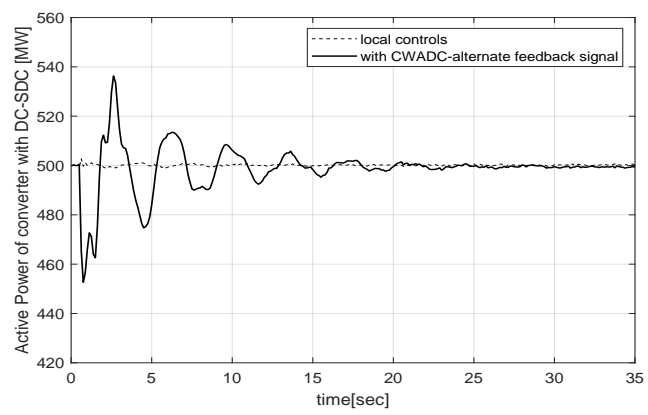


Fig. 15. Alternate Feedback-DC Output.

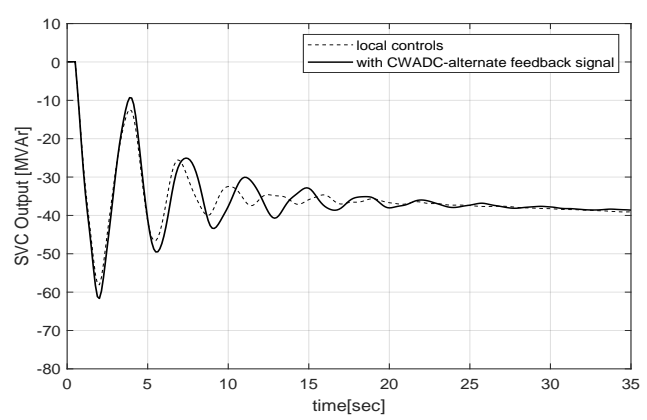


Fig. 16. Alternate Feedback-Reactive Power Output of SVC.

C. Incorporation of Delays

The implementation of the CWADC requires data to be transmitted from the selected PMU locations to the coordinated controller. As detailed in [8], [24], it is possible that the data traveling through different communication channels reach the same destination at different times. This is because every channel may have a different latency associated with it due to varying network configurations and congestion. Test results obtained in [8] for a real-time damping control designed for the WECC indicate that the total delay, that includes the switching delay of about 11ms, is on average 82 ms with a maximum value recorded at 113 ms. Hence, in this research, non-linear simulations are performed by adding an implicit random delay, that lies between 25-100ms, to the wide-area signals. The gains obtained using the primary set of feedback

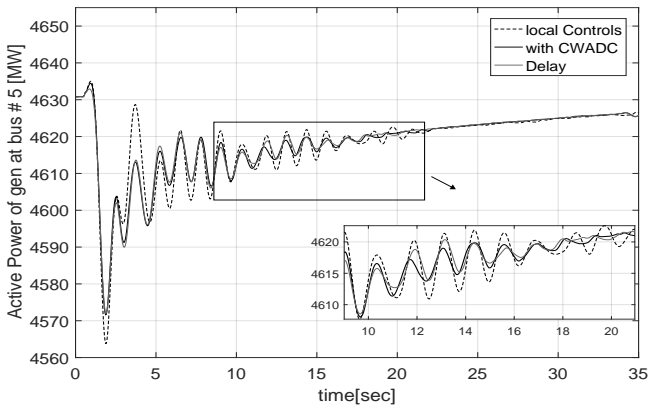


Fig. 17. Active Power of Generator #5 with Delay of 0.1s.

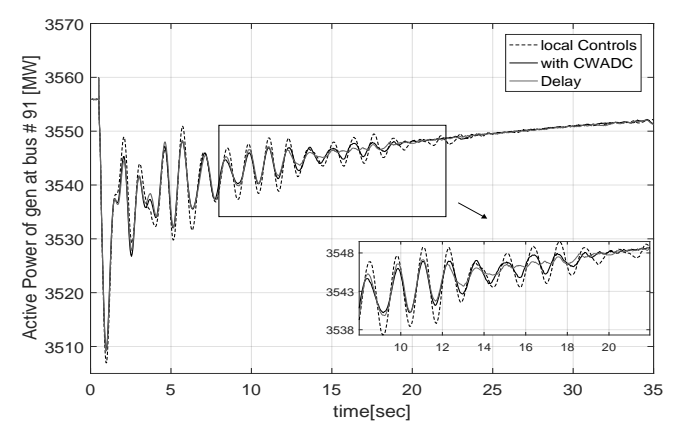


Fig. 18. Active Power of Generator #91 with Delay of 0.08s.

signals are used for the simulations. It can be observed from Figs. 17-18, that when the CWADC suffers a communication delay, the performance of the controller degrades slightly, but it still performs better than the local controllers. However, if the delays are too large, it is acceptable to revert to the local controllers. This would remain the case until the latency in the wide-area signals is small enough to ensure a positive effect on the oscillation damping.

D. Large Disturbance Analysis

By subjecting the test system to large disturbances, the actual non-linear behavior of the system can be observed, and the performance of the CWADC assessed accordingly. For the large disturbance simulated here, the network is subjected to a 100ms three-phase fault at bus #105 at t=0.5sec. The improved performance realized by employing CWADC is evident in the results of the transient simulation shown in Figs. 19-22, which depict the active powers of four generators present at bus #5 (a generating unit in Canada), bus #26 (a generating station in Montana), bus #76 (a generating station in Southern California), and bus #91 (a generating unit in Northern California); see Fig. 3 for the bus locations. It is clear from Figs. 19-22 that in the presence of CWADC, the system experiences significantly smaller swings.

E. Robustness Comparison

To demonstrate the benefits associated with the proposed method, a comparison is made with another control scheme for a specific operating point that lies inside the designed polytope

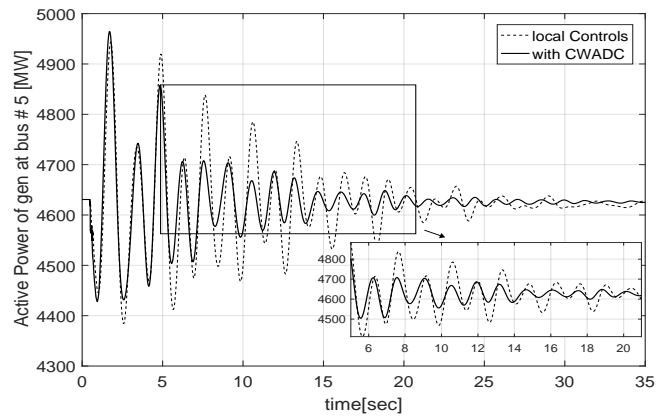


Fig. 19. Fault Analysis-Active Power of Generator #5.

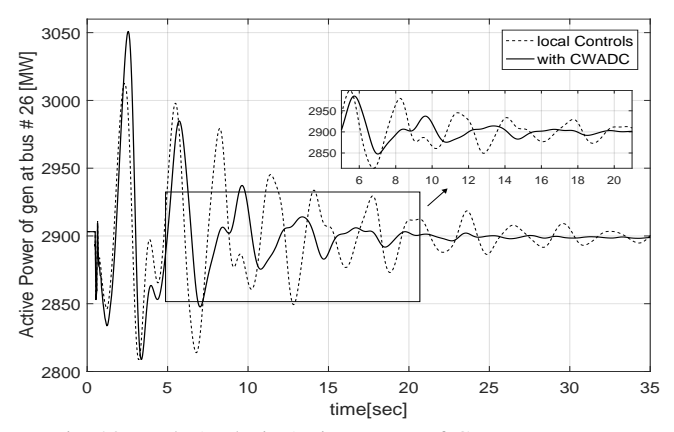


Fig. 20. Fault Analysis-Active Power of Generator #26.

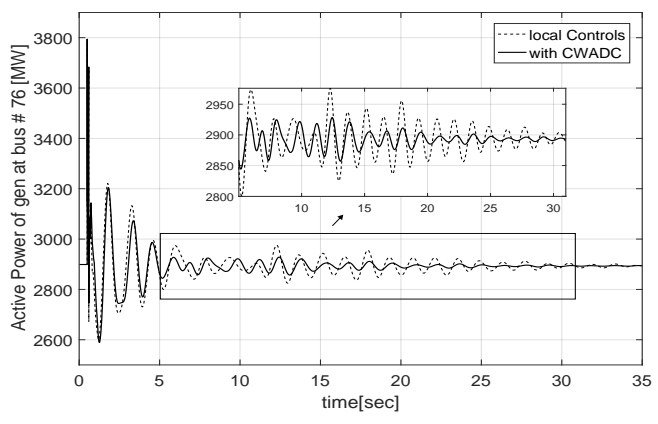


Fig. 21. Fault Analysis-Active Power of Generator bus#76.

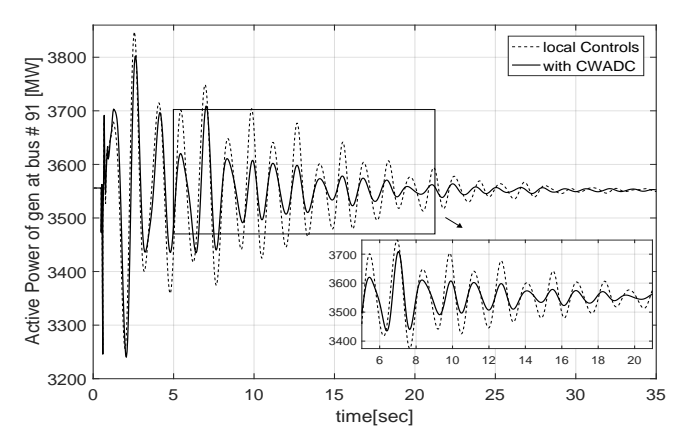


Fig. 22. Fault Analysis-Active Power of Generator #91.

but is not one of its vertices. The load at bus #69 is increased by 100 MW at t=0.5sec. The analysis is performed by designing two additional non-polytopic controls using LQR: a) the first non-polytopic control corresponds to a controller that is designed for vertex v_1 , i.e. base OC, b) the second non-polytopic control corresponds to a controller that is designed for the simulated disturbance, i.e., increase in load at bus 69 by 100 MW, by treating it as a *known* operating point.

The active powers of two generators, i.e., gen at bus #5 and bus #91 which have maximum participation in the least damped modes for this operating point are shown in Figs. 23-24. From the two plots, it can be seen that the first non-polytopic controller performs poorly as it is designed for the base OC. The performance of the second non-polytopic controller is comparable to that of the CWADC; however, designing that controller requires prior knowledge of the OC, which is not likely to happen in reality. Thus, this comparison illustrates the benefit of using a polytopic control, as a single controller can guarantee the desired damping effect for all the OCs lying inside the polytope.

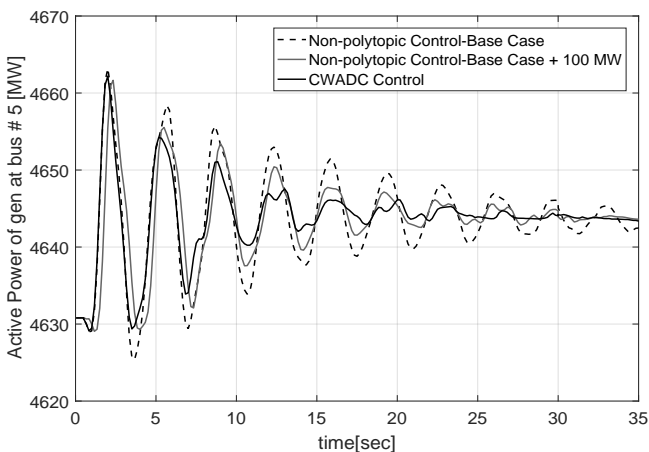


Fig. 23. Comparative Analysis-Active Power of Generator #5.

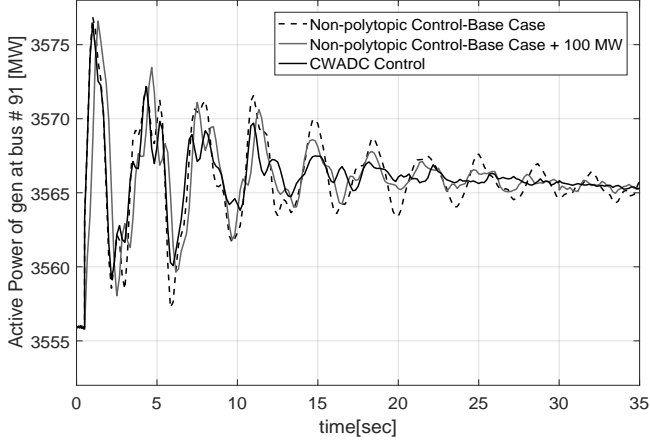


Fig. 24. Comparative Analysis-Active Power of Generator #91.

VI. DISCUSSIONS

The success of the single polytopic controller design for a wide range of OCs depends on two factors: a) diversity of the OCs, and b) number of OCs considered. If the OCs are very diverse, or the number of OCs that are intended to be combined into a single polytope are too many, the controller gain matrix

generated after solving the LMI-based control problem can have potentially large magnitudes of gains. Similarly, trying to move the closed-loop poles to the left by a significant margin or an incongruous selection of the weights for H_2 and H_∞ controls during the creation of the polytope can also lead to excessively large controller gains. These scenarios should be avoided as they can lead to controller output saturation.

The proposed approach offers an advantage over adaptive control design schemes as no processing time is required for control selection and actuation depending on the system's OC. Since all the controller parameters are obtained using off-line case studies and can be stored for online operations, there will be no delay in accessing the controller data. Furthermore, the synthesized control is composed of gains only, as compared to other higher-order controllers that have large numbers of control parameters (such as [7] and [25]). Hence, the designed control is more appropriate for real-time applications, as it is computationally tractable and does not require knowledge of various control parameters.

VII. CONCLUSIONS

In this paper, the design of a simple, yet efficient method for designing wide-area damping controllers is proposed for mitigating LFOs using an enhanced SMA and LMI-based polytope. The approach facilitates the coordination of existing controls in the system, thereby enabling them to overcome their inability to act cohesively on the basis of local measurements, to damp the oscillation modes. Additionally, to ensure robustness, the coordinated controller can switch between primary and alternate sets of feedback signals in case of failure of the measurement device and/or communication channel. The proposed method serves as a good fit for actual implementation by power system utilities since its design requires much less computational burden as compared to other non-linear control designs. This is also promising since the resulting controller is a single gain matrix capable of enhancing the damping of all the cases lying inside the polytope, while not modifying/disrupting the existing controller parameters.

Modal analysis and time domain simulations are performed to test the viability of the proposed control. The practical issue of delay in the control signals is analyzed by adding variable latency to different control signals. Simulation results suggest that use of this scheme can be advantageous for providing additional damping to the critical oscillatory modes despite the presence of reasonable delays. As sampling rate and communication latency can affect the performance of widearea controllers, future work will report the results that are obtained when the delays are incorporated in the design of the CWADC. The authors also intend to utilize a machine learning based approach to leverage the applicability and computational time of the proposed method. Specifically, the aim would be to utilize the historical data for assessing the large number of possible operating scenarios at a fraction of time required by the traditional approaches.

REFERENCES

 Q. Liu, V. Vittal, and N. Elia, "LPV supplementary damping controller design for a thyristor controlled series capacitor (tcsc) device," *IEEE Trans. Power Syst.*, vol. 21, no. 3, pp. 1242–1249, 2006.

- [2] T. Wang, A. Pal, J. S. Thorp, Z. Wang, J. Liu, and Y. Yang, "Multi-polytope-based adaptive robust damping control in power systems using cart," *IEEE Trans. Power Syst.*, vol. 30, no. 4, pp. 2063–2072, 2014.
- [3] T. Wang, A. Pal, J. S. Thorp, and Y. Yang, "Use of polytopic convexity in developing an adaptive interarea oscillation damping scheme," *IEEE Trans. Power Syst.*, vol. 32, no. 4, pp. 2509–2520, 2017.
- Trans. Power Syst., vol. 32, no. 4, pp. 2509–2520, 2017.
 [4] H. Ni, G. T. Heydt, and L. Mili, "Power system stability agents using robust wide area control," *IEEE Trans. Power Syst.*, vol. 17, no. 4, pp. 1123–1131, 2002.
- [5] G. Sánchez-Ayala, V. Centeno, and J. Thorp, "Gain scheduling with classification trees for robust centralized control of psss," *IEEE Trans. Power Syst.*, vol. 31, no. 3, pp. 1933–1942, 2015.
- [6] A. Chakrabortty, "Wide-area damping control of power systems using dynamic clustering and TCSC-based redesigns," *IEEE Trans. Smart Grid*, vol. 3, no. 3, pp. 1503–1514, 2012.
- [7] S. Zhang and V. Vittal, "Design of wide-area power system damping controllers resilient to communication failures," *IEEE Trans. Power* Syst., vol. 28, no. 4, pp. 4292–4300, 2013.
- [8] B. J. Pierre, F. Wilches-Bernal, D. A. Schoenwald, R. T. Elliott, D. J. Trudnowski, R. H. Byrne, and J. Neely, "Design of the Pacific DC Intertie wide area damping controller," *IEEE Trans. Power Syst.*, 2019.
- [9] T. Nguyen and R. Gianto, "Optimisation-based control coordination of PSSs and FACTS devices for optimal oscillations damping in multimachine power system," *IET Gener., Transmiss. & Distrib.*, vol. 1, no. 4, pp. 564–573, 2007.
- [10] Y. Li, C. Rehtanz, S. Ruberg, L. Luo, and Y. Cao, "Wide-area robust coordination approach of HVDC and FACTS controllers for damping multiple interarea oscillations," *IEEE Trans. Power Del.*, vol. 27, no. 3, pp. 1096–1105, 2012.
- [11] A. Pal, J. S. Thorp, S. S. Veda, and V. Centeno, "Applying a robust control technique to damp low frequency oscillations in the WECC," *Int.l J.Elect. Power & Energy Syst.*, vol. 44, no. 1, pp. 638–645, 2013.
- [12] R. Preece, J. V. Milanovic, A. M. Almutairi, and O. Marjanovic, "Damping of inter-area oscillations in mixed AC/DC networks using WAMS based supplementary controller," *IEEE Trans. Power Syst.*, vol. 28, no. 2, pp. 1160–1169, 2013.
- [13] P. Gupta, A. Pal, C. Mishra, and T. Wang, "Design of a coordinated wide area damping controller by employing partial state feedback," in *Power & Energy Soc. General Meeting (Atlanta)*, 2019 IEEE PES, pp. 1–5, IEEE, 2019.
- [14] V. Vittal and J. D. McCalley, Power system control and stability. John Wiley & Sons, 3 ed., 2019.
- [15] GE Technical Staff, "PSLF user's manual." General Electric International, Inc., 2019.
- [16] J. C. Doyle, "Guaranteed margins for lqg regulators," *IEEE Trans. Automatic Control*, vol. 23, no. 4, pp. 756–757, 1978.
- [17] P. Gahinet, A. Nemirovski, A. J. Laub, and M. Chilali, "LMI control toolbox: For use with MATLAB (MathWorks)," 1995.
- [18] J. Ma, T. Wang, X. Gao, S. Wang, and Z. Wang, "Classification and regression tree-based adaptive damping control of inter-area oscillations using wide-area signals," *IET Gener., Transmiss. & Distrib.*, vol. 8, no. 6, pp. 1177–1186, 2014.
- [19] G. C. Verghese, I. Perez-Arriaga, and F. C. Schweppe, "Selective modal analysis with applications to electric power systems, part II: The dynamic stability problem," *IEEE Trans. Power App. and Syst.*, no. 9, pp. 3126–3134, 1982.
- [20] A. Pal and J. S. Thorp, "Co-ordinated control of inter-area oscillations using SMA and LMI," in 2012 IEEE PES Innovative Smart Grid Technologies (ISGT), pp. 1–6, 2012.
- [21] A. Beghi, "An application of selective modal analysis to tokamak modeling and control," *IEEE Trans. Control Syst. Technol.*, vol. 9, no. 4, pp. 574–589, 2001.
- [22] ²²013 WECC path reports." WECC Staff Western Electricity Coordinating Council. Avaiable: https://www.wecc.biz/Reliability/TAS_ PathReports_Combined_FINAL.pdf, 2013.
- [23] DSA Tools Technical Staff, "SSAT model manual." PowerTech Labs Inc., 2017.
- [24] Y. Zhou, J. Liu, Y. Li, C. Gan, H. Li, and Y. Liu, "A gain scheduling wide-area damping controller for the efficient integration of photovoltaic plant," *IEEE Trans. Power Syst.*, vol. 34, no. 3, pp. 1703–1715, 2018.
- [25] W. Qiu, V. Vittal, and M. Khammash, "Decentralized power system stabilizer design using linear parameter varying approach," *IEEE Trans. Power Syst.*, vol. 19, no. 4, pp. 1951–1960, 2004.